DOI: 10.13009/EUCASS2022-4433
9TH EUROPEAN CONFERENCE FOR AERONAUTICS AND SPACE SCIENCES (EUCASS)

REST HF-10 test case: Synthesis of the Contributions for the Simulation of Excited Methane Flames under Real Gas Conditions

Thomas Schmitt[3] (thomas.schmitt@centralesupelec.fr)
Roland Kaess[1] (roland.kaess@ariane.group)

Roland Behr[1] (roland.behr@ariane.group)
Stefan Koeglmeier[1] (stefan.koeglmeier@ariane.group)
Oliver Knab[1] (oliver.knab@ariane.group)
[1]Ariane Group, Robert-Koch-Straße 1, 82024 Taufkirchen, Germany

Tim Horchler[2] (tim.horchler@dlr.de)
Jan van Schyndel[3] (jan.vanschyndel@dlr.de)
Justin S. Hardi[3] (justin.hardi@dlr.de)
[2]Deutsches Zentrum für Luft- und Raumfahrt (DLR), Bunsenstraße 10, 37073 Göttingen, Germany
[3]Deutsches Zentrum für Luft- und Raumfahrt (DLR), Im Langen Grund 1, 74239 Hardthausen, Germany

David Marchal[4] (david.marchal@centralesupelec.fr)
Sébastien Ducruix[4] (sebastien.ducruix@centralesupelec.fr)
[4]Laboratoire EM2C, CNRS, CentraleSupelec, Université Paris-Saclay, 3 rue Joliot Curie, 91190 Gif-sur-Yvette, France

Aurélie Nicole[5] (aurelie.nicole@onera.fr)
Luc-Henry Dorey[5] (luc-henry.dorey@onera.fr)
[5]DMPE, ONERA, Université Paris-Saclay, F- 91123 Palaiseau, France

Abstract

The REST (Rocket Engine Stability iniTiative) test case HF-10 is a numerical test case for the calculation of a liquid oxygen - methane ($LOx - CH_4$) coaxial flame at 100 bar. The participants of the 4th REST modelling workshop from both industrial and scientific institutions were invited to use their respective commercial or in-house codes and models to simulate the test case. One steady state and three excited calculations were requested. The approaches used by the participants were LES, DES and U-RANS with different chemistry models and different numerical schemes. Hence, comparing the results is expected to unveil the influence of these aspects. Important differences in flame structure and dynamics are visible and highlight the particularities and capabilities of the modelling.

1. Introduction

Liquid propellant rocket engine combustion instabilities are a major concern in the developments of rocket engines. Such instabilities lead to pressure oscillations of extremely high amplitudes which affect the physical phenomena in the chamber leading to collapse of the thermal boundary layer and eventually to damage or destruction of the hardware (Figure 1). There are numerous examples of programs being affected by such problems and the predication of such instabilities remains a challenging goal [1].

The driving mechanism behind these instabilities is an interaction of the combustion process with the combustion chamber acoustics. Therefore, a sound understanding of both the acoustics and the combustion process as well as their interaction with the flow field are essential and subject to ongoing research.

DOI: 10.13009/EUCASS2022-4433

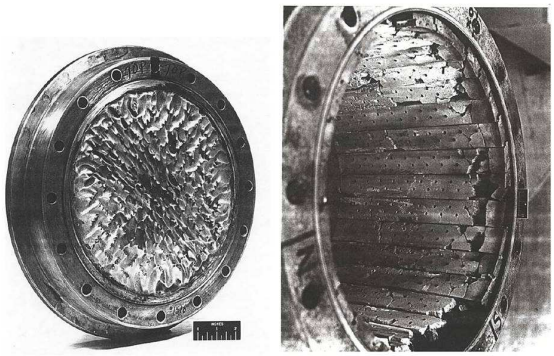

Figure 1: Hardware damaged by combustion instability (Image source: NASA)

The Rocket Engine Stability iniTiative (REST) is a cooperative network of French and German partners from industry, research institutes, and academia on the topic of rocket combustion instability. The members share their progress and findings in regular scientific workshops. Additionally, modelling workshops are held to benchmark the predictive capabilities of partners' numerical tools. In these modelling workshops, test cases are defined and the participants calculate them with their respective methods of choice. In this way, perspectives on the advantages, strengths, limitations and drawbacks of the different approaches can be gained.

The present publication deals with the so-called test case HF-10 from the fourth such workshop in 2019 which is based on virtual demonstrators defined in the frame of a former German Collaborative Research Centre, DFG SFB TRR 40[1] [12]. This test case was designed to assess the capabilities of the different approaches to model a single rocket combustor flame under dynamic excitation. The aim was to specifically have a view on the different CFD methods being used in the REST community. The dynamic excitation of the flame was chosen to be in the form of modulation of the inlet mass flow rate of propellant. This kind of excitation presents a well-defined basis for comparison. The propellant combination of liquid oxygen and methane (LOx-CH_4) was chosen due to its current relevance to Europe's space program.

2. Test case description

The configuration consists of a LOx - CH_4 coaxial injector. The coaxial injector and its dimensions are detailed in Figure 2a. LOx is injected through the inner injector, while gaseous CH_4 is injected from the annular pipe. The 300-mm length combustion chamber is sketched in Figure 2b. Its cross-section is hexagonal with each face being periodic with the opposite side. The outlet boundary conditions should be non-reflecting. Walls are considered as adiabatic and both no-slip or wall-law slipping boundary conditions can be used depending on the applied methodology.

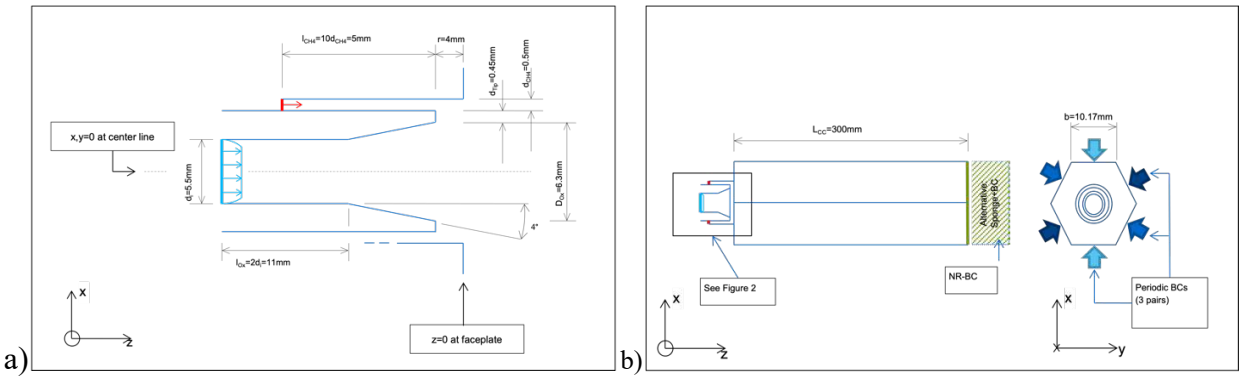

Figure 2: Sketch of the computational domain. (a) Coaxial injector (b) Chamber.

Injection conditions are indicated in Table 1. Turbulent fluctuations with an intensity of 5% are added at inlets. Four cases are considered in this work. One is the steady flame configuration, referenced as NM (non-modulated). Mass flow rate modulations are imposed for the three other cases. For case FM (fuel modulated), a 10% amplitude

[1] Deutsche Forschungsgemeinschaft, Sonderforschungsbereich Transregio 40

DOI: 10.13009/EUCASS2022-4433

modulation at 5 kHz is imposed at the fuel inlet, while the modulation is imposed on oxygen for cases OM (oxidizer modulated). Two frequencies are considered for the latter case: 1 kHz and 5 kHz. All the cases are summarized in Table 2.

Table 1: Cases and corresponding injection conditions. $\dot{m}_{CH4}$ and $\dot{m}_{O2}$ are the methane and oxygen mass flow rates, respectively. T_{CH4} and T_{O2} are the methane and oxygen injection temperatures. The chamber pressure is referenced as p_{ch}.

$\dot{m}_{CH4}$ [kg/s]	T_{CH4} [K]	$\dot{m}_{O2}$ [kg/s]	T_{O2} [K]	p_{ch} [MPa]
0.136	231	0.46	100	10

Table 2: Detail of the selected cases. NM, FM and OM stand for Non-Modulated, Fuel-Modulated and Oxidizer-Modulated, respectively. $\Delta\dot{m}_{CH4}$ and $\Delta\dot{m}_{O2}$ are the mass flow rate modulation amplitudes at the methane and oxygen inlet. Their corresponding frequencies are noted f_{mod}^{CH4} and f_{mod}^{O2}.

Case	$\Delta\dot{m}_{CH4}$	f_{mod}^{CH4}	$\Delta\dot{m}_{O2}$	f_{mod}^{O2}
NM	0	-	0	-
FM	10 %	5 kHz	0	-
OM-5kHz	0	-	10 %	5 kHz
OM-1kHz	0	-	10 %	1 kHz

3. Overview of Contributions

In this paper, contributions to the test case from the following four members of the REST research group are compared and contrasted:

- ArianeGroup at Ottobrunn (AG-OTN), Germany, with the ANSYS CFX solver [11]
- German Aerospace Center (DLR), Institutes of Aerodynamics and Flow Technology, Göttingen, and of Space Propulsion, Lampoldshausen, with the DLR-TAU code [9]
- Laboratoire EM2C, CNRS located at CentraleSupélec, Université Paris-Saclay, France, with the AVBP solver from CERFACS [10]
- ONERA at Palaiseau, France, with the CEDRE in-house solver [8]

The numerical frameworks used by the contributors are detailed in Table 3. The main difference between the numerical frameworks relies on the choice of the numerical method: AG-OTN and ONERA use an Unsteady-Reynolds averaged Navier-Stokes simulation (U-RANS) approach while DLR and EM2C perform Delayed Detached-Eddy Simulation (DES) and Large-Eddy Simulation (LES), respectively. The concept of DES is to combine RANS, near the walls, and LES in the domain. The choice of the combustion model also differs between the participants. EM2C and ONERA assume equilibrium chemistry, DLR solves a near-equilibrium flamelet model, while an Eddy Dissipation Concept (EDC) model coupled with a 1-step irreversible Arrhenius mechanism is solved in AG-OTN's framework. Finally, a large variability exists between the methods in terms of CPU cost, which ranges from 10 000 h to 520 000 h for 10 ms of physical time. More details about the models, meshes and numerical methodologies can be found in the contributors dedicated EUCASS papers [8,9,10,11].

Table 3: Numerical frameworks used by the participants. Details of the meshes and models and associated references may be found in each contributor EUCASS article [8,9,10].

	AG-OTN	DLR	EM2C	ONERA
EUCASS Article	[11]	[9]	[10]	[8]
Solver	ANSYS CFX	TAU [4]	AVBP [6,7]	CEDRE [2,3]
Type	U-RANS	DDES [5]	LES	U-RANS
Type of mesh elements	Hexa	Hexa	Tetra	Hybrid
Number of grid points	$5.8\ 10^6$	$12.3\ 10^6$	$2.7\ 10^6$	$2.3\ 10^6$

DOI: 10.13009/EUCASS2022-4433

Turbulence / sub-grid scale model	SST	Smagorinsky	WALE	k-ω model – SST Menter
Combustion model	EDC / 1 step Arrhenius	Near-equilibrium flamelet model	Pdf-equilibrium	Relaxation to equilibrium
Number of species / reactions	4 species 1 reaction	22 species 49 reactions	7 species	9 species
Numerical schemes		low-Ma-corrected MAPS+ upwind Jameson-type dual time stepping	Two Steps Taylor-Galerkin C (TTGC)	Multi-slope MUSCL / HLLC GMRES
Spatial order	1 on scalars / 2 on momentum	2	3	2
Temporal order	1	1	3	1
Num. stabilization / limiter	None	None	Artificial viscosity	Hybrid limiter
Real-gas equation of state	Table based on NIST (O_2 only)	SRK	SRK	SRK (O_2, CH_4 only)
CPU for 10 ms	10 kh	520 kh	50 kh	223 kh

4. Case NM

The case without modulation (case NM) is analyzed in this section. Results are first presented in term of longitudinal slices and profiles of mean quantities. Instantaneous fields are then exposed for the LES and DES solvers.

4.1 Longitudinal cuts of mean temperature and heat release rate in the y-z plane

Longitudinal slices of mean temperature for case NM are shown in Figure 3. All the simulations show a similar flame topology: the cold oxygen flow is surrounded by a diffusion flame, attached to the injector lips. The flow features a sudden spreading just after the injector exit, at z≈15 mm, which is due to the confinement of the flame. Further downstream, the flame features a nearly straight evolution with a highly stratified flow, stucked between the methane and oxygen streams, up to the end of the cold inner flow. Finally, the temperature field becomes nearly homogeneous up to the end of the chamber.
Even if the shape of the flame is similar for all the cases, quantitative results strongly differ depending on the numerical framework used. The flame length, defined by taking the position of the end of the cold region, colored blue, is almost twice as long (≈150 mm vs ≈80 mm) in U-RANS simulations (AG-OTN & ONERA) than for LES/DES (DLR & EM2C). Also, the maximum mean temperature in the first half of the domain (z<150 mm) is larger in RANS simulations than LES/DES. The much larger temperature obtained by AG-OTN may be due to the simple, one-step, irreversible chemistry used in their solver. The initial spreading angle predicted by EM2C is larger than that by DLR, suggesting a quicker inner jet destabilization.

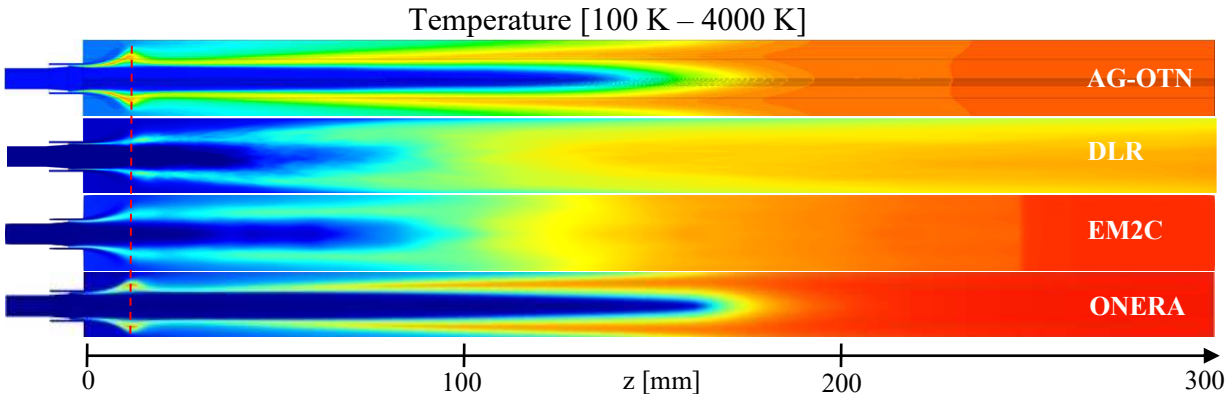

Figure 3: Case NM. Longitudinal slices of mean temperature (y-z plane).

DOI: 10.13009/EUCASS2022-4433

To complement the temperature visualizations, heat release rate distributions are shown in Figure 4. Large differences exist between the contributions. All the simulations consistently indicate a much higher reaction rate near the injector, where the strain rate is high, than in the rest of the chamber. This heat release decreases after the initial sudden flame opening (around 15 mm from the injection plane). Aside from the length difference mentioned earlier, EM2C results present a large region of homogeneous heat release rate not so clearly observed with the other approaches. Finally, the peak value of heat release rate reached in the domains differ between the models. It is the largest for EM2C and ONERA, both using an equilibrium chemistry scheme.

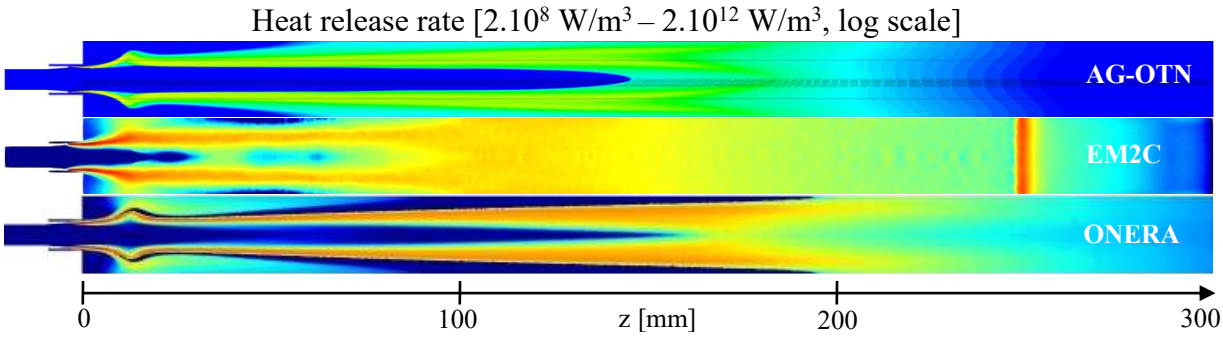

Figure 4: Case NM. Longitudinal slices of mean heat release rate (y-z plane). The red zone at 250 mm for EM2C is due to the presence of a dissipation patch before the outlet.

4.2 Longitudinal and radial profiles of mean variables

A more direct comparison between the simulations was performed by plotting longitudinal profiles of cross-averaged mean temperature, oxygen mass fraction, density and heat release rate in Figure 5. Temperature profiles qualitatively follow the same axial progression for all the simulations up to 150 mm, with a quasi-linear increase from ≈500 K to ≈2500 K. The slope then diminishes for LES (EM2C) and DES (DLR), while it is suddenly augmented for RANS simulations (AG-OTN & ONERA). In general, LES and DES show a similar trend while RANS simulations follow another evolution.

Focusing on LES and DES, a difference is observed in the near injector region (z<50 mm) with a lower temperature for DLR. This is also observed in oxygen mass fraction and density, which are lower and higher, respectively, for DLR compared with EM2C. It suggests a longer intact core for DLR. Further downstream, the two solvers are in reasonable agreement.

The difference between ONERA and AG-OTN might be due to the combustion model, predicting a higher temperature for AG-OTN, but the slopes are comparable. There is also a very good agreement between these two solvers for the oxygen mass fraction between 40 mm and 170 mm. The cause of the peak at z<30 mm for ONERA can not yet be explained.

Finally, AG-OTN, EM2C and ONERA obtained heat release rates of the same order of magnitude, which is a satisfactory point given the importance of proper heat release rate prediction. But, given the first order impact of this quantity for the prediction of thermoacoustic gain, the factor 2 measured between the contributions represents a large remaining level of uncertainty.

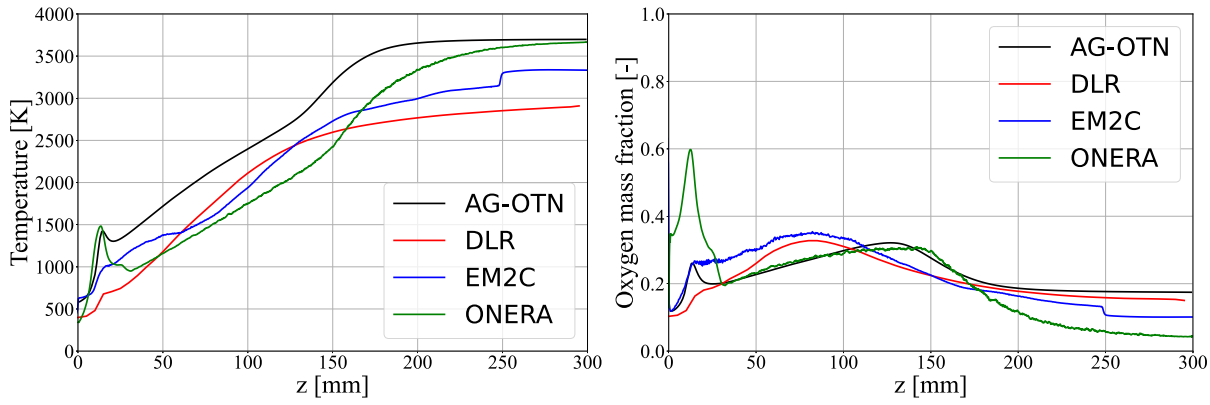

DOI: 10.13009/EUCASS2022-4433

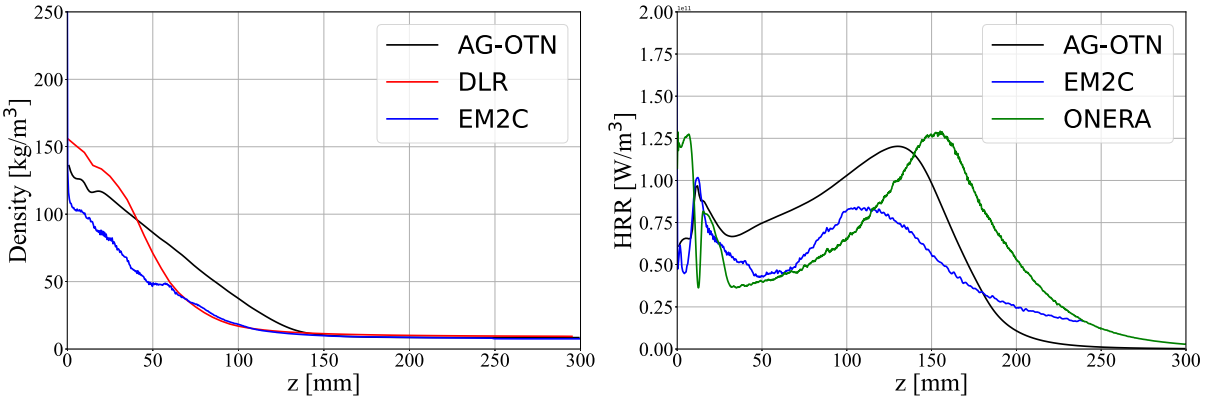

Figure 5: Case NM. Longitudinal profiles of cross-plane averaged temperature, oxygen mass fraction, density and heat release rate.

Additional radial profiles are provided in Figure 6 for EM2C, DLR and AG-OTN in the near injector region. A large departure between the simulations is observed for z=10 mm and z=20 mm. While maximum temperatures are similar, the flame brush thickness is much larger for EM2C than DLR. Further downstream, profiles from LES and DES are close to each other. On the contrary, the temperature profile predicted by AG-OTN strongly departs from the others: the flame is still open at 100 mm and the maximum temperature is much higher. These results are confirmed by the oxygen mass fraction profiles plotted in Figure 7. Finally, axial velocity plotted in Figure 8 shows large departure between the simulations. This is particularly significant for z=10 mm between LES and DES. The annular stream remains weakly destabilized for DLR, in contrary to EM2C.

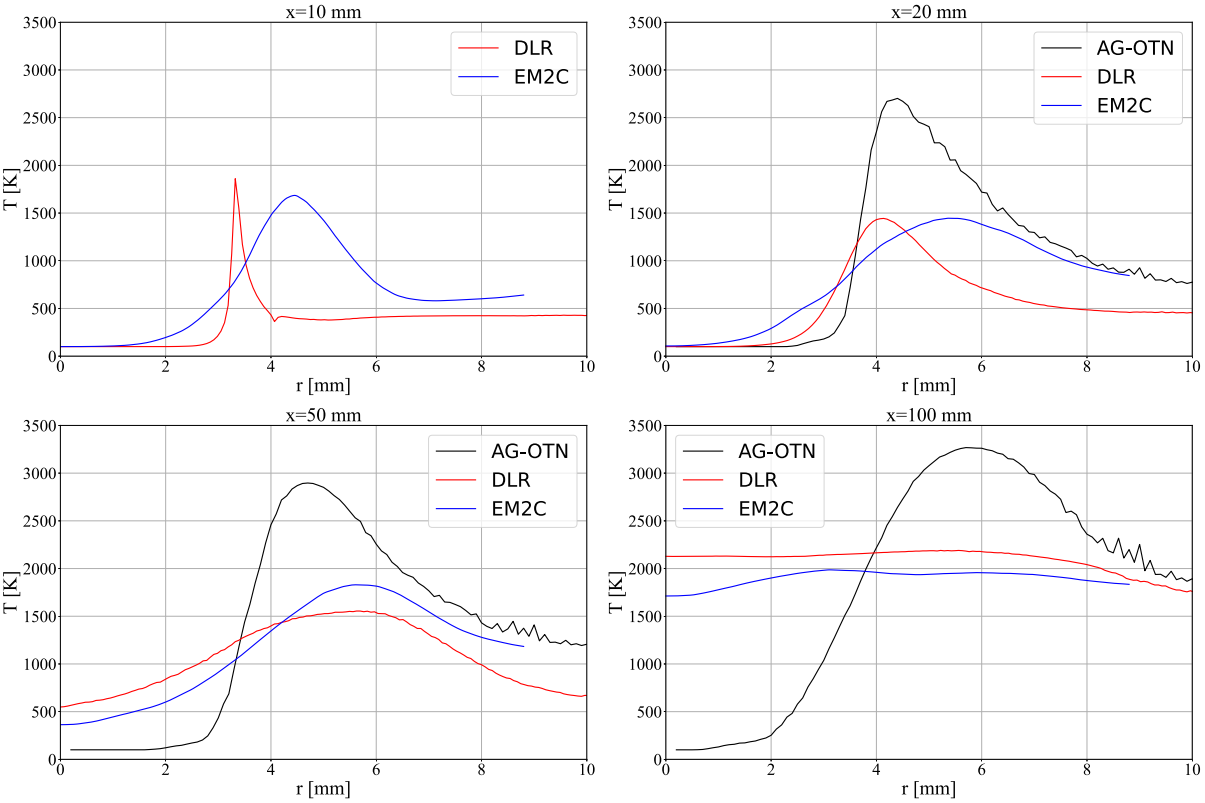

Figure 6: Case NM. Radial profiles of mean temperature.

DOI: 10.13009/EUCASS2022-4433

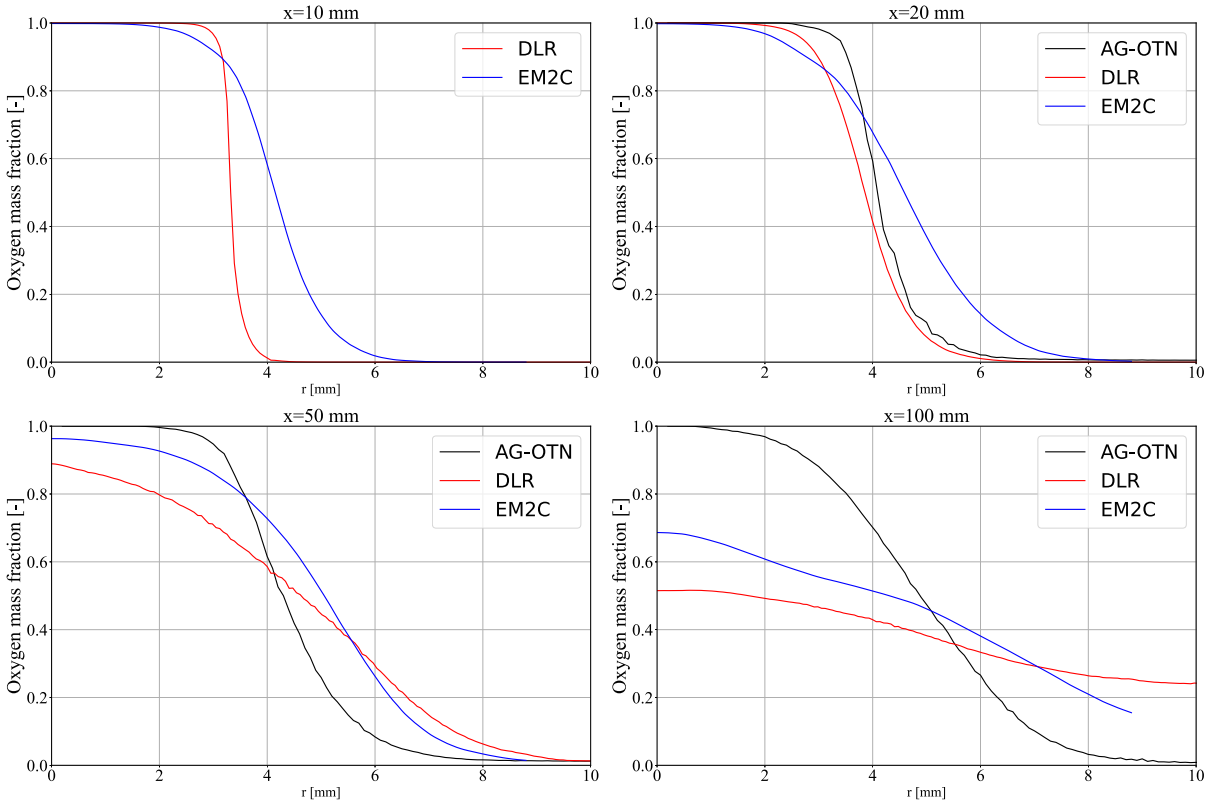

Figure 7: Case NM. Radial profiles of mean oxygen mass fraction.

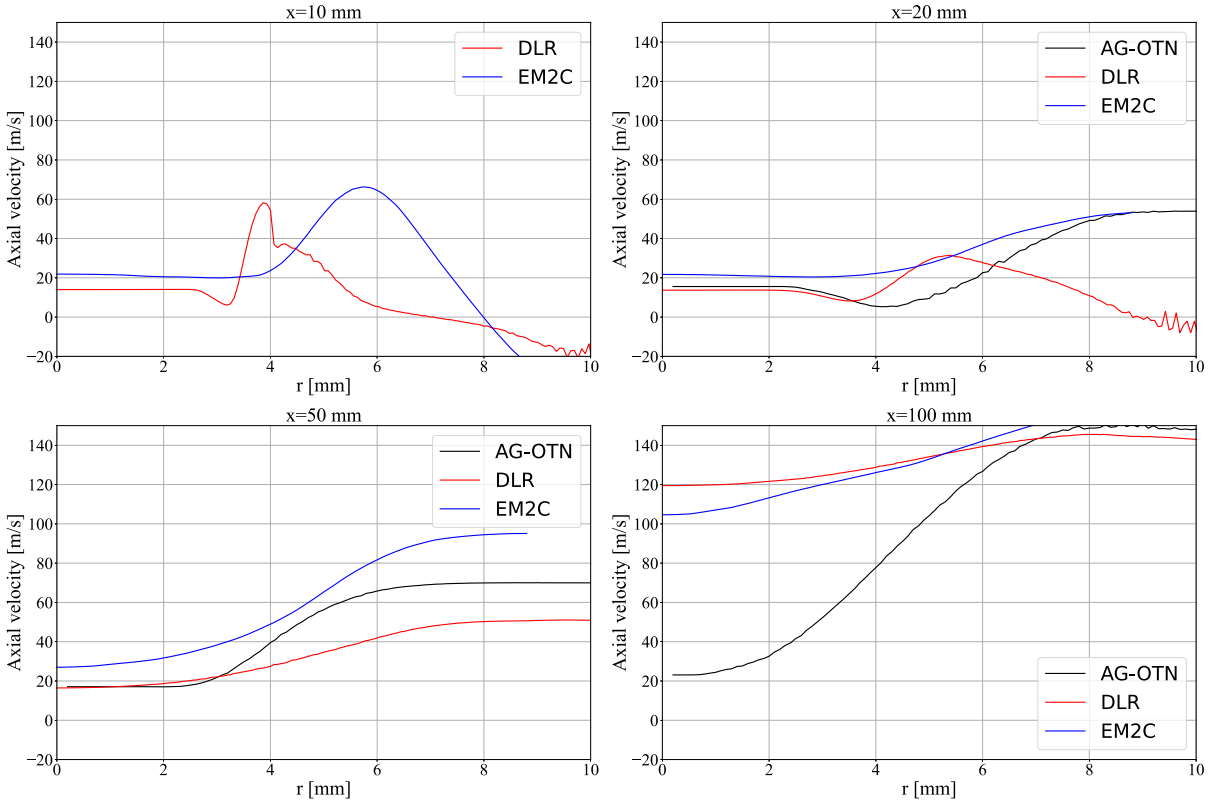

Figure 8: Case NM. Radial profiles of mean axial velocity.

DOI: 10.13009/EUCASS2022-4433

4.3 Instantaneous fields for DES and LES simulations

Longitudinal slices of instantaneous density and temperature are offered in Figure 9. The high-density inner jet is destabilized earlier in the EM2C simulation than in DLR simulation. Nevertheless, both jets have similar penetration into the chamber, explaining the same flame length between the two simulations. It is expected that these differences may be attributed to different choices of meshing strategies (hexa vs tetra) and sub-grid scale closures (Smagorinsky vs WALE) between the two groups. This aspect should be studied in more detail in the future.

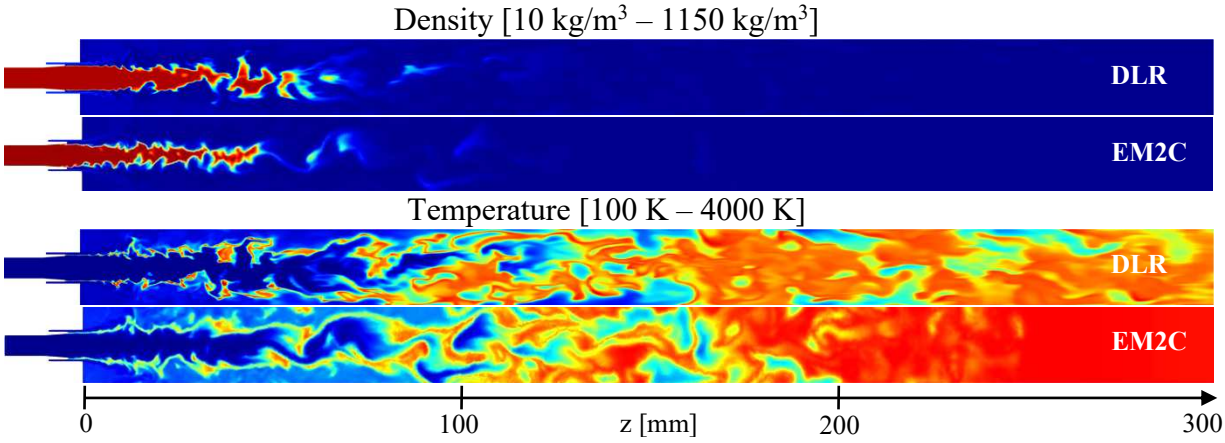

Figure 9: Case NM. Longitudinal slices (x-y plane) of density and temperature.

5. Case FM

This section now concentrates on case FM, for which the fuel (annular methane injection) is modulated at 5 kHz with an amplitude of 10% of the mean mass flow rate.

5.1 Longitudinal cuts of mean temperature and heat release rate in the y-z plane

For all the contributions, modulating the annular flow has little impact in the mean flow. To illustrate, the mean temperature and heat release rate are shown in Figure 10 and Figure 11, respectively. The latter are close to those obtained for case NM (Figure 3 and Figure 4).

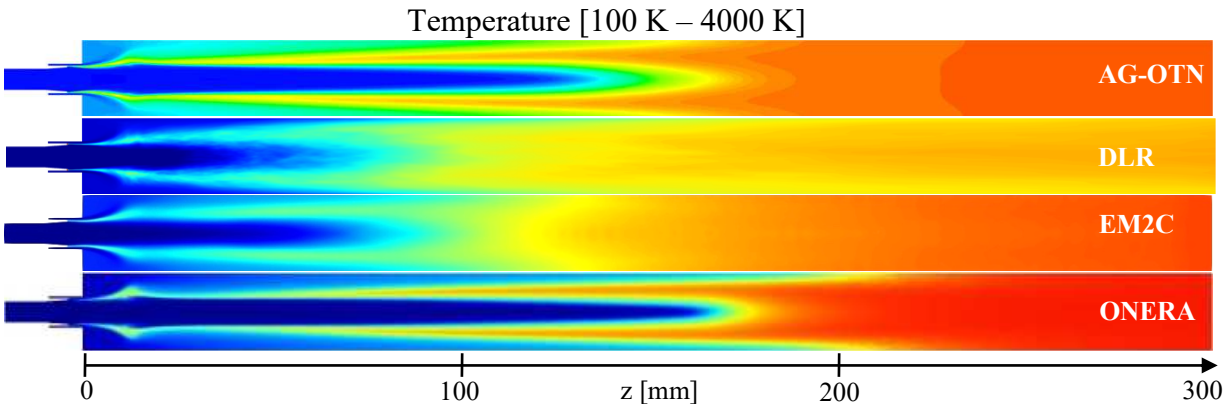

Figure 10: Case FM. Longitudinal slices of mean temperature (y-z plane).

DOI: 10.13009/EUCASS2022-4433

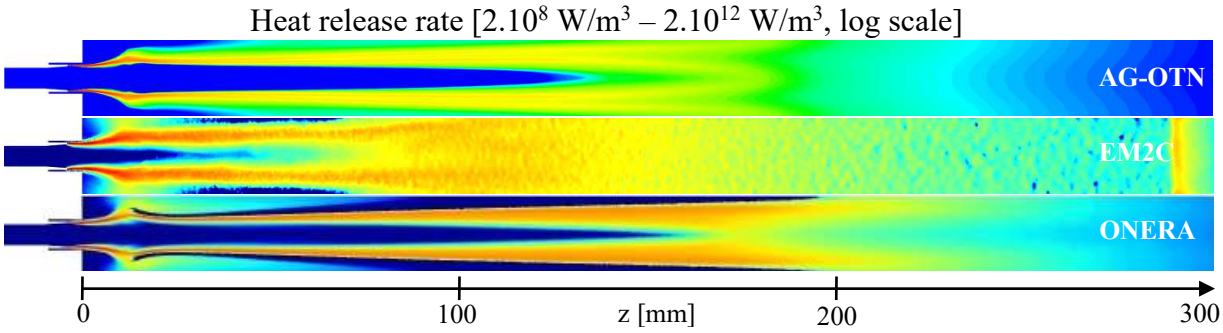

Figure 11: Case FM. Longitudinal slices of mean heat release rate (y-z plane).

More precisely, it is shown in Figure 12 that the flame is slightly shortened once modulated. This behavior is common to all the simulations. However, the heat release rate is increased for z<100 mm for EM2C, while it remains little affected for AG-OTN and ONERA.

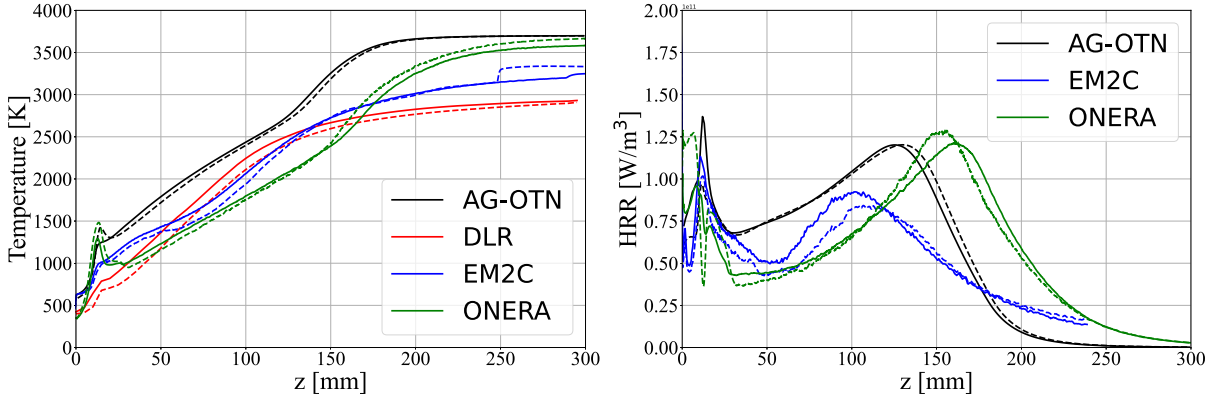

Figure 12: Case FM. Longitudinal profiles of cross-plane averaged temperature and heat release rate. The dashed lines show the profiles without modulation (NM).

5.2 Longitudinal cuts of phase averaged fields in the y-z plane

Phase averaged fields of temperature (Figure 13) reveal an oscillation of the flame front induced by the annular modulation. Harmonic perturbations propagate from the injector exit up to z≈40 mm. The phenomenon is observed for all the simulations. Perturbations seem to propagate further downstream for EM2C compared with AG-OTN and ONERA. As it was observed for NM, local values of temperature strongly differ between the models, it is the warmest for AG-OTN and the coolest for EM2C. Red dashed lines have been super-imposed on Figure 13 to allow for a qualitative comparison of the axial location of a crest between the simulations. The lines are arbitrarily positioned to correspond to AG-OTN results. AG-OTN and EM2C are in good agreement, for both phases presented here.

Similar observations can be made on the heat release rate phase-averaged field plotted in Figure 14. Heat release rate oscillations are induced by the inlet modulation but given the large discrepancies between the models it is expected flame responses will differ between the models.

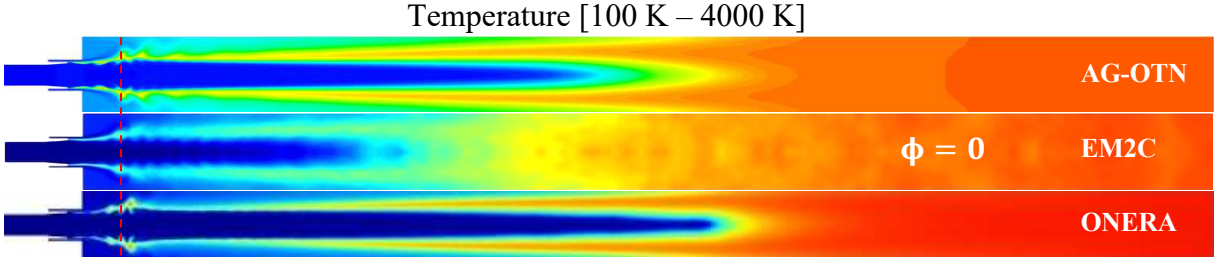

DOI: 10.13009/EUCASS2022-4433

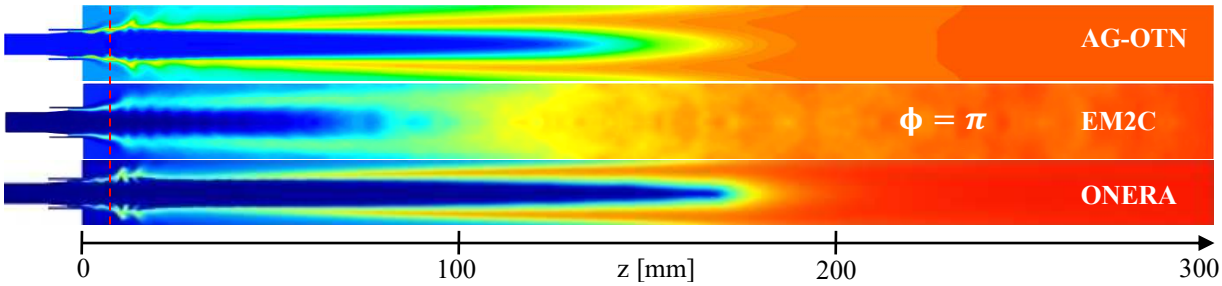

Figure 13: Case FM. Longitudinal slices of phase-averaged temperature (y-z plane) for two distinct phases.

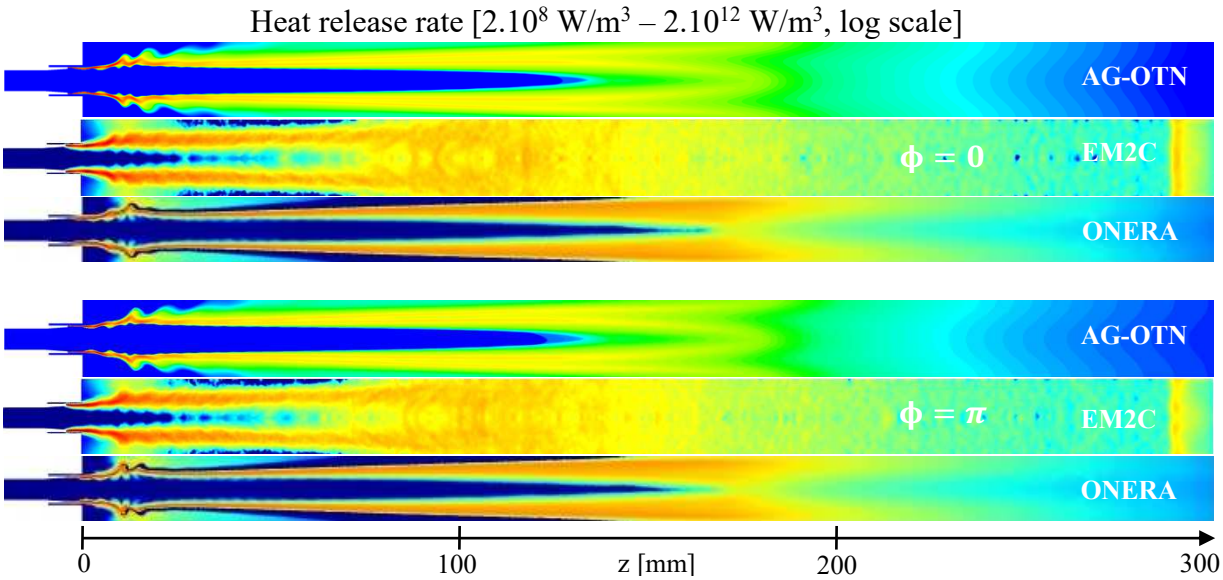

Figure 14: Case FM. Longitudinal slices of phase-averaged heat release rate (y-z plane) for two distinct phases.

6. Case OM-5kHz

The inner, LOX flow is modulated in this section. As for case FM, the modulation amplitude is 10 % at a frequency of 5 kHz.

6.1 Longitudinal cuts of mean temperature and heat release rate in the y-z plane

Average fields of temperature and heat release rate are provided in Figure 15 and Figure 16. As for case FM, they are little impacted by the inner flow modulation, except for AG-OTN which now shows a flame topology close to DLR and EM2C. This latter result – only observed for this case - is surprising and requires further investigations.

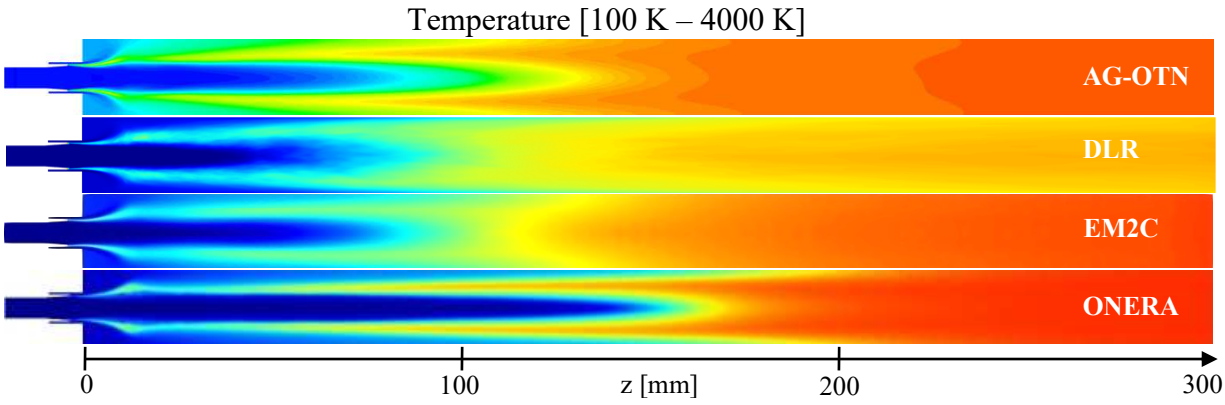

Figure 15: Case OM-5kHz. Longitudinal slices of mean temperature (y-z plane).

DOI: 10.13009/EUCASS2022-4433

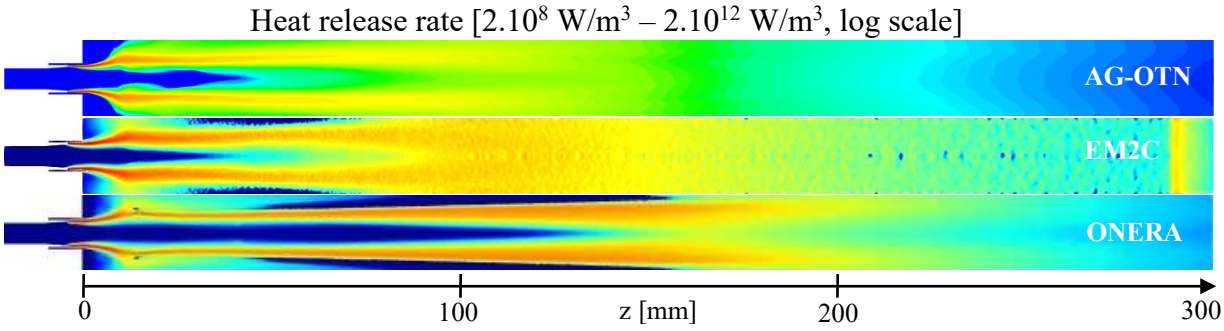

Figure 16: Case OM-5kHz. Longitudinal slices of mean heat release rate (y-z plane).

As for FM, the flame length is reduced by the modulation (see for example the temperature profiles in Figure 17). This reduction is stronger for U-RANS simulations, especially for AG-OTN. Consequently, the corresponding heat release profiles are importantly modified (Figure 17).

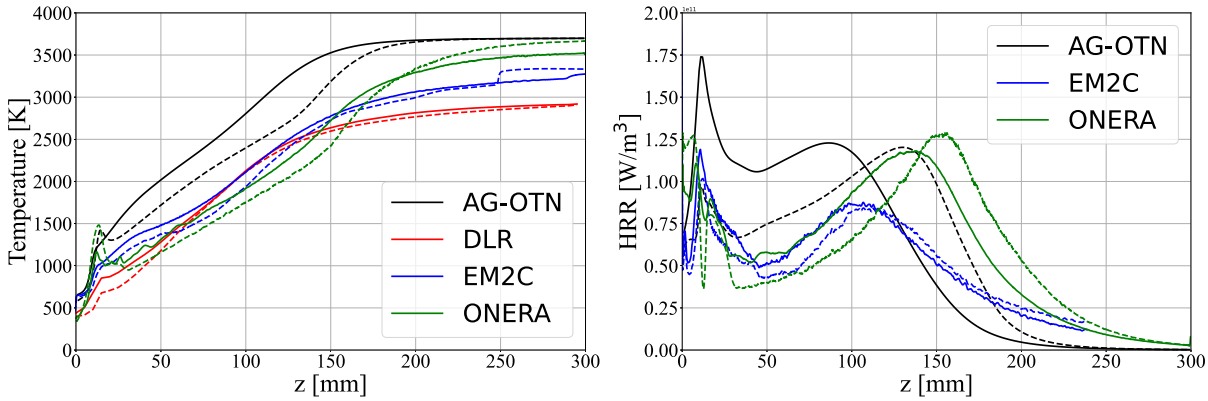

Figure 17: Case OM-5kHz. Longitudinal profiles of cross-plane averaged temperature and heat release rate. The dashed lines show the profiles without modulation (NM).

6.2 Longitudinal cuts of phase averaged fields in the y-z plane

Phase averaged results (Figure 18) show a close dynamic for AG-OTN and EM2C, with near injector perturbations located at a similar position. Simulation from ONERA shows large differences with the other participants in terms of topology and propagation of the perturbations downstream in the chamber.

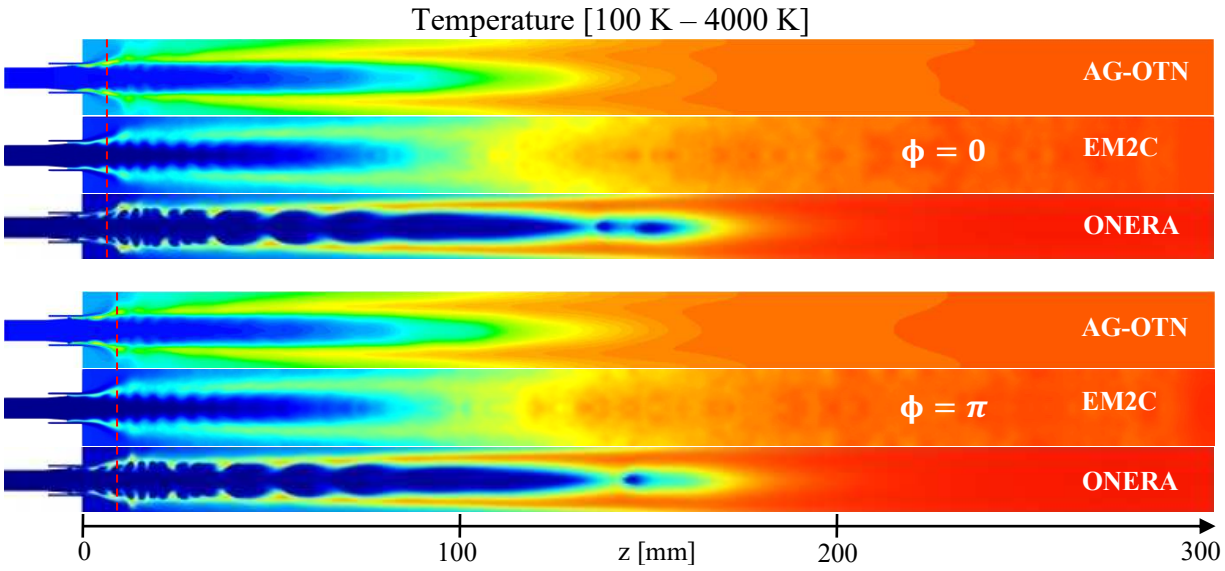

Figure 18: Case OM-5kHz. Longitudinal slices of phase-averaged temperature (y-z plane) for two distinct phases.

DOI: 10.13009/EUCASS2022-4433

As it could be qualitatively seen from Figure 19, all the simulations produce local variations of heat release rate near the injector. They propagate further in the domain for ONERA.

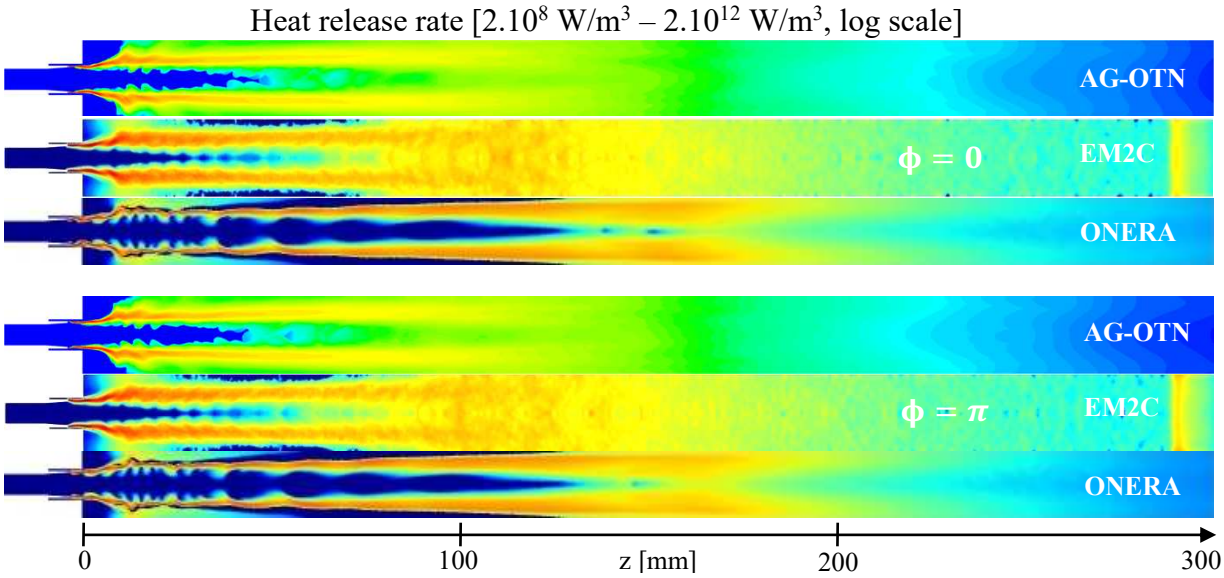

Figure 19: Case OM-5kHz. Longitudinal slices of phase-averaged heat release rate (y-z plane) for two distinct phases.

7. Case OM-1kHz

The last test case featuring a modulated LOx injection at 1kHz with an amplitude of 10% is provided in this section.

7.1 Longitudinal cuts of mean temperature and heat release rate in the y-z plane

Mean fields of temperature and heat release rate are plotted in Figure 20 and Figure 21. Again, they are both very similar to the non-modulated case, for all the simulations. A small reduction of the flame length is observed for all the calculations in Figure 22. This reduction of the flame length is associated with an increase of the heat release rate for AG-OTN and EM2C.

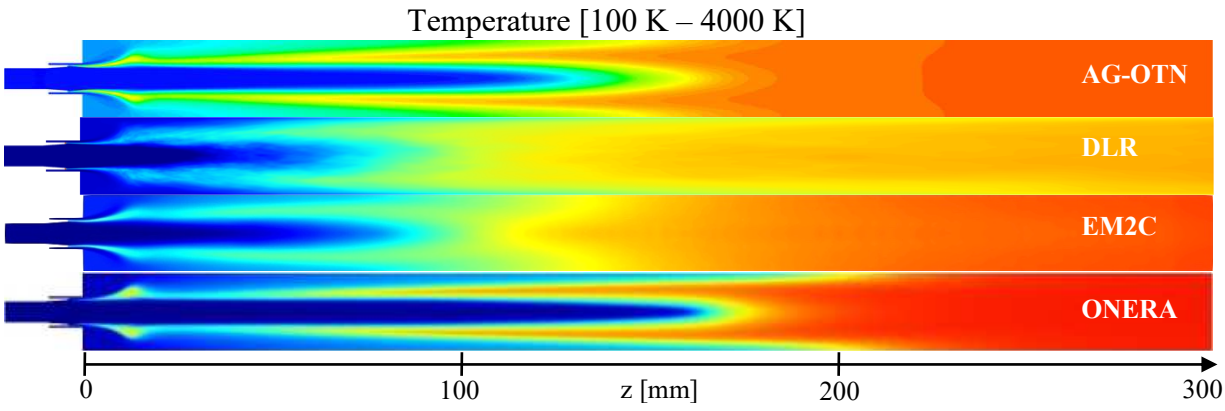

Figure 20: Case OM-1kHz. Longitudinal slices of mean temperature (y-z plane).

DOI: 10.13009/EUCASS2022-4433

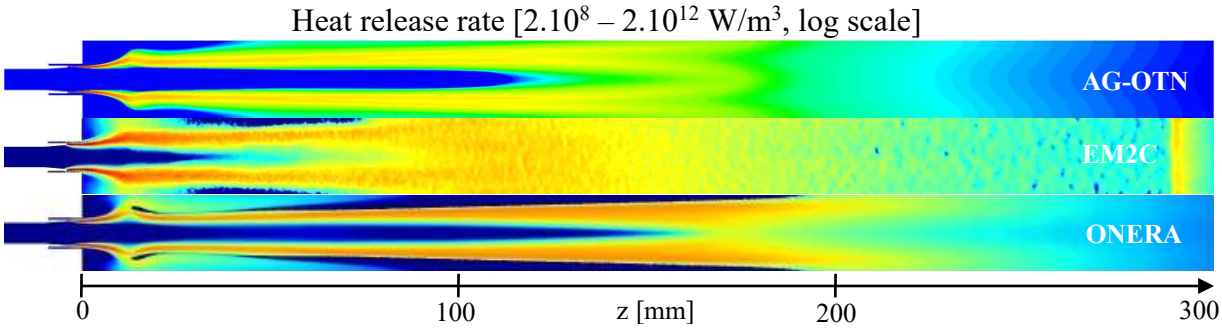

Figure 21: Case OM-1kHz. Longitudinal slices of mean heat release rate (y-z plane).

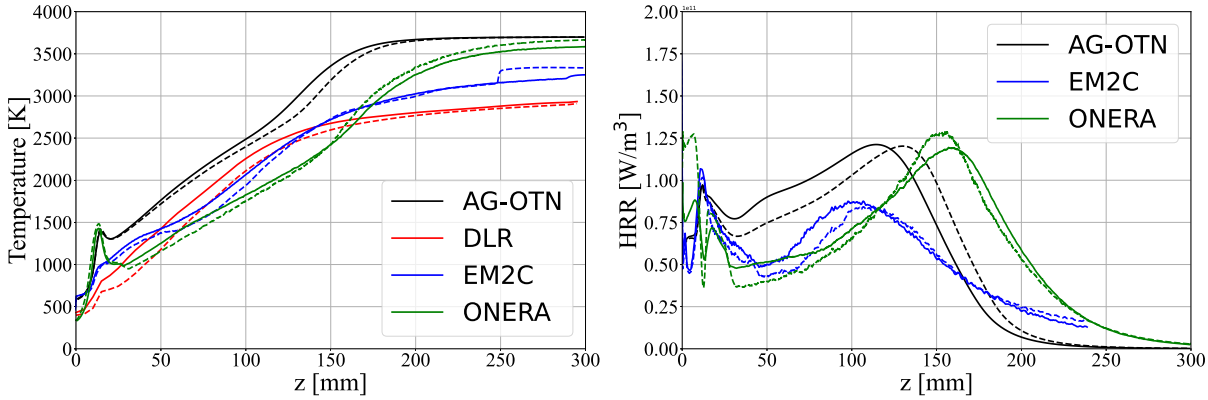

Figure 22: Case OM-1kHz. Longitudinal profiles of cross-plane averaged temperature and heat release rate. The dashed lines show the profiles without modulation (NM).

7.2 Longitudinal cuts of phase averaged fields in the y-z plane

Flow dynamics is now discussed in term of phase-averaged fields. Compared with the cases at 5 kHz, induced oscillations now penetrate further downstream in the chamber. This is observed for all the simulations. The position of the first crest is similar for the 3 participants, but differences appear further downstream. The wavelength of the inner jet seems larger for EM2C than AG-OTN and ONERA, whereas the latter two are no longer in phase. The kinematic deformation induced by the modulation is also present in the heat release rate field in Figure 24.

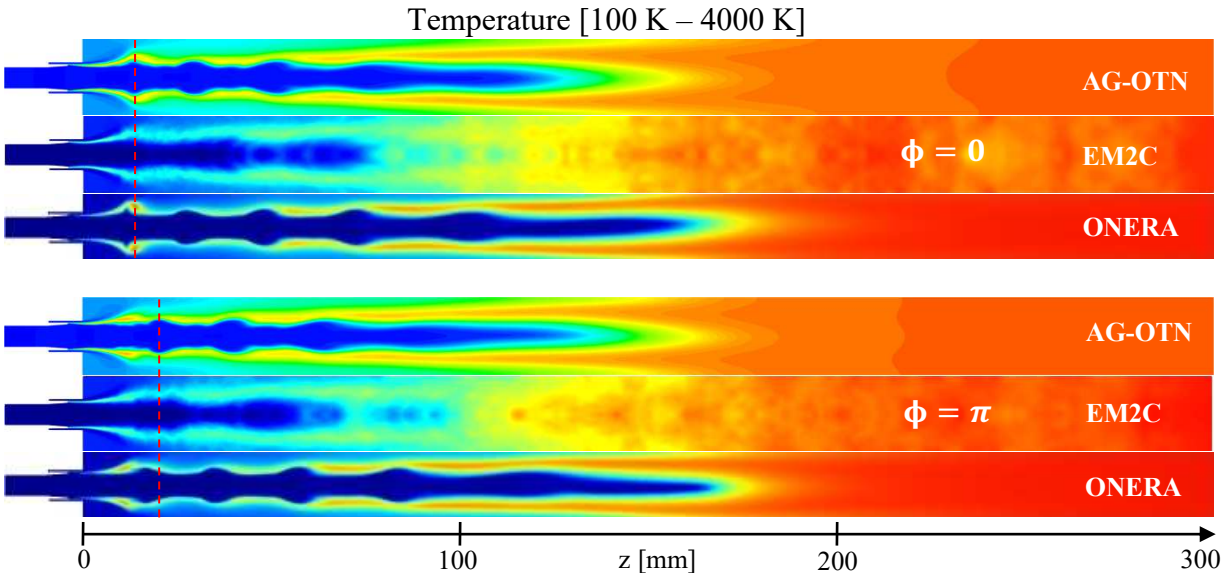

Figure 23: Case OM-1kHz. Longitudinal slices of phase-averaged temperature (y-z plane) for two distinct phases.

DOI: 10.13009/EUCASS2022-4433

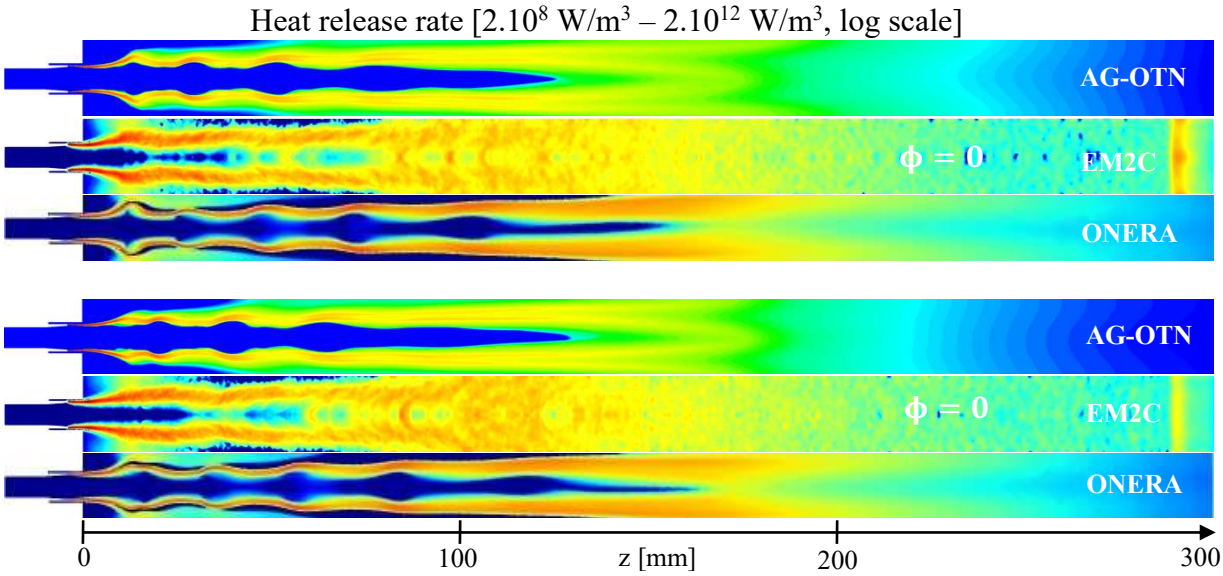

Figure 24: Case OM-1kHz. Longitudinal slices of mean heat release rate (y-z plane).

8. Conclusions and perspectives

Numerical simulations of a LOx/CH_4 coaxial injector operating at 100 bar have been performed by different groups in the context of the HF-10 test-case from the REST (Rocket Engine Stability iniTiative) working group. HF-10 features 4 different calculations: a steady state (NM) and 3 excited cases for which modulations are imposed at the annular or the central inlet of the coaxial injector (cases FM and OM, respectively).

Four participants from the REST research group contributed to this test case: 1) ArianeGroup at Ottobrunn (AG-OTN), Germany, with the ANSYS CFX solver; 2) German Aerospace Center (DLR) at Göttingen and Lampoldshausen, Germany, with the DLR-TAU code; 3) Laboratoire EM2C, CNRS located at CentraleSupélec, Université Paris-Saclay, France, with the AVBP solver from CERFACS; 4) ONERA at Palaiseau, France, with the CEDRE in-house solver. AG-OTN and ONERA use an Unsteady-Reynolds averaged Navier-Stokes simulation (U-RANS) approach while DLR and EM2C perform Delayed Detached-Eddy Simulation (DES) and Large-Eddy Simulation (LES), respectively.

For case NM, all the contributions predict a similar flame topology, featuring a turbulent diffusion flame anchored to the lips of the injector. However, quantitative predictions may strongly differ between the simulations:

- The flame length is approximatively 2 times longer for U-RANS compared with LES and DES.
- The local flame temperature is higher for RANS than LES/DES in the stratified region, along the oxygen core.
- Heat release fields show large local disparities between the participants. However, there is a qualitative agreement once averaged along transverse planes.

It is found that the largest differences could be attributed to the numerical framework: LES/DES or U-RANS. The simple combustion model used by AG-OTN seems to explain most of the differences (higher temperature, heat release rate) with ONERA in the RANS context. The largest departure between LES and DES simulations occur at the injector exit, where simulations from DLR feature a longer intact core and a sharper flame brush than those from E2MC. It may be attributed to different choices of meshing strategies and sub-grid scale closures between the two groups. All these aspects need more investigations to obtain indisputable conclusions.

Once modulated, all simulations generally produce a comparable flame dynamic, with oscillations propagating from the injector along the flame. For all the simulations, the modulation produces a slight shortening of the flame, but has virtually no impact on the flame topology. Most of the differences between the contributors are thus inherited from the base flow without modulation, with a much longer flame length for U-RANS than LES/DES. The resulting perturbations are generally in phase between EM2C and AG-OTN.

From this comparison between the contributions, recommendations for future work are proposed:

- The research group should concentrate on case NM as it is the baseline for the other cases under modulation.
- LES or DES – which are expected to be more accurate - should be used to improve RANS models.

DOI: 10.13009/EUCASS2022-4433

References

[1] AIAA. Liquid Rocket Engine Combustion Instability, Yang, V.; Anderson, W. and Zarchan, P. 1995

[2] Refloch A., Courbet B., Murrone A., Villedieu P., Laurent C., Gilbank P., Troyes J., Tessé L., Chaineray G., Dargaud J.B., Quémerais E. and Vuillot F. (2011). CEDRE Software. Aerospace Lab, vol. 2.

[3] Gaillard, P., Giovangigli, V., and Matuszewski, L. (2016) A diffuse interface Lox/hydrogen transcritical flame model. Combustion Theory and Modelling 20 pp 486 - 520.

[4] D. Schwamborn, T. Gerhold, and R. Heinrich. The DLR-TAU-Code: Recent applications in research and industry. In *Proceedings of the European Conference on Computational Fluid Dynamics (ECCOMAS)*, 2006.

[5] Philippe R Spalart, Shur Deck, Michael L Shur, Kyle D Squires, M Kh Strelets, and Andrei Travin. A new version of detached-eddy simulation, resistant to ambiguous grid densities. *Theoretical and computational fluid dynamics*, 20(3):181, 2006.

[6] T. Schönfeld and M. Rudgyard. Steady and unsteady flows simulations using the hybrid flow solver AVBP. *AIAA Journal*, 37(11):1378–1385, 1999.

[7] T. Schmitt. Large-eddy simulations of the Mascotte test cases operating at supercritical pressure. *Flow, Turbulence and Combustion*, 105:159–189, 2020.

[8] A. Nicole, L.H. Dorey. REST HF10 test case: Simulation of combustion instabilities induced by flow rate modulations with diffuse interface modelling. In *9th European Conference for Aeronautics and Aerospace Sciences (EUCASS), 2022.*

[9] T. Horchler, S. Fechter, J. van Schyndel and M. Oschwald. REST HF-10 Test Case: Numerical Simulation of a Single Coaxial LOX-CH4 Injector with Forced Mass Flow Oscillations Using the DLR TAU-Code. In *9th European Conference for Aeronautics and Aerospace Sciences (EUCASS) , 2022.*

[10] T. Schmitt, D. Marchal, S. Ducruix, B. Cuenot. REST HF-10 test case: Large-Eddy Simulations using the AVBP solver. In *9th European Conference for Aeronautics and Aerospace Sciences (EUCASS), 2022.*

[11] R. Kaess, S. Koeglmeier, R. Behr, O. Knab. REST HF-10 test case: URANS Simulations of Excited Methane Flames under Real Gas Conditions. In *9th European Conference for Aeronautics and Aerospace Sciences (EUCASS),, 2022.*

[12] D. Eiringhaus, H. Riedmann, O. Knab, O. J. Haidn. Full-Scale Virtual Thrust Chamber Demonstrators as Numerical Testbeds within SFB-TRR 40. In 2018 Joint Propulsion Conference*, 2018.*